Type-II GaInAsSb/InP Uniform Absorber High Speed Uni-Traveling Carrier Photodiodes

Akshay M. Arabhavi, Rimjhim Chaudhary, Ralf Flückiger, Diego Marti, Sara Hamzeloui, Filippo Ciabattini, Wei Quan, Martin Leich, Olivier Ostinelli, and C. R. Bolognesi, *Fellow, IEEE*

***Abstract*—We report uniform Type-II GaInAsSb/InP UTC-PDs, and compare their performance to devices fabricated with GaAsSb uniform and graded (composition and doping) absorbers of the same thickness. The quaternary UTC-PDs show a transit limited bandwidth of 274 GHz in contrast to 107 and 185 GHz for uniform and graded GaAsSb absorber UTC-PDs. Because the uniform quaternary and ternary UTC-PDs only differ in their absorber material, the findings conclusively demonstrate enhanced transport in GaInAsSb. Performance comparison to GaInAs-based devices from the literature suggest that GaInAsSb is a superior absorber material for $\lambda = 1.55\ \mu$m high-speed photodetectors. Additionally, the external responsivity of the GaInAsSb UTC-PDs (0.094 A/W) is ∼34% higher than the GaAsSb PDs (0.070 A/W). This is the first demonstration of a quaternary GaInAsSb absorber in UTC-PDs.**

***Index Terms*—Uni-traveling carrier photodiodes (UTC-PDs), responsivity, InP, GaInAsSb, GaAsSb, transit limited bandwidth (f_{T}).**

I. Introduction

UNITRAVELLING carrier photodiodes (UTC-PDs) achieve wider bandwidths than conventional PIN-PDs because the former only involve transport of fast moving carriers (electrons) through the absorber and collector layers, while the response time of photo-generated holes is effectively reduced to the order of the dielectric relaxation time of holes in the *p*-type absorber layer. This avoids the long tail response associated with hole drift transport taking place in PIN-PDs.

Ishibashi *et al*. demonstrated 3-dB bandwidths of 310 GHz in UTC-PDs with a GaInAs absorber layer and compositional grading to facilitate electron transfer to an InP drift collector [1]. Since their demonstration, UTCs found a rich variety of applications in wireless transmission, THz generation, etc. [2]–[4].

Whenever electrons must be transferred from a GaInAs absorber (or the base layer in an HBT) to an InP collector, a central consideration is the grading scheme between GaInAs and InP because of the $\Delta E_{\mathrm{C}} = 0.25$ eV conduction band discontinuity between the two materials. Regardless of the selected scheme, e.g. compositional step-grading [1] or a chirped superlattice [5], under high excitation the traveling space charge of electrons eventually collapses the electric field due to depleted donors in the collector, re-exposes the ΔE_{C} to InP, and limits the ultimate device performance for high-drive conditions.

In light of these considerations, some of us [6] demonstrated UTC-PDs using a GaAsSb absorber in 2005, exploiting the fact that the conduction band edge of $\mathrm{GaAs_{0.51}Sb_{0.49}}$ is higher than that of InP ("Type-II" alignment), favoring electron transport even under flat-band conditions. The operating principle of a Type-II UTC-PD was successfully demonstrated but with lower bandwidths than possible with a GaInAs absorber of the same thickness because of a lower electron mobility (diffusivity) in the $\mathrm{GaAs_{0.51}Sb_{0.49}}$ alloy in comparison to $\mathrm{Ga_{0.47}In_{0.53}As}$ [6, 7]. This imposes a serious limitation on the overall performance of Type-II UTC-PDs in terms of the trade-off between PD responsivity (scaling with $\sim W_{\mathrm{A}}$) and the absorber diffusion delay (scaling with $\sim {W_{\mathrm{A}}}^2$). Calculations by Tea *et al*. indicate that GaAsSb shows a lower mobility than GaInAs because the former is characterized by a relatively low Γ-L conduction band intervalley separation with a significant population of the indirect low-mobility satellite valleys, even under modest electron injection levels [7]. Furthermore, the GaAsSb L-valley conduction band is lower than in InP, resulting in a blocking Type-I band discontinuity which impedes the L-valley electron flow from GaAsSb to InP. Despite comparatively lower bandwidths, simulations by Dyson *et al*. [8] suggest that Type-II GaAsSb UTC-PDs would offer performance advantages with respect to GaInAs-based devices, especially under high optical drive conditions. It is therefore of interest to determine whether the electron transport properties of GaAsSb absorbers can be engineered to be competitive with those of GaInAs *while* maintaining the advantages of a Type-II band alignment to InP.

We recently showed [9, 10] that a GaInAsSb base layer enables higher cutoff frequencies in InP/GaInAsSb DHBTs by raising the L-valley with respect to GaAsSb (and reducing its population and eliminating the L-valley blocking effects at the B/C heterojunction with InP), and by improving electron mobility in the base layer. Starting from $\mathrm{GaAs_{0.51}Sb_{0.49}}$ lattice-matched to InP, it is readily understood that incorporating In-in the GaAsSb matrix must be accompanied by a reduction of the Sb- mole fraction to maintain lattice-matching between GaInAsSb and InP. Consideration of the Γ-L valley separation

Manuscript received October 16, 2020; revised November 23, 2020 and December 3, 2020; accepted December 5, 2020. Date of publication December 9, 2020; date of current version April 2, 2021. This work was supported by SNF Project under Grant 200021_188725. *(Corresponding author: C. R. Bolognesi.)*

The authors are with ETH Zurich, 8092 Zürich, Switzerland (e-mail: akshaym@mwe.ee.ethz.ch; rchaudhary@mwe.ee.ethz.ch; ralff@mwe.ee.ethz.ch; diego.marti@mwe.ee.ethz.ch; hasara@mwe.ee.ethz.ch; fciabattini@mwe.ee.ethz.ch; wquan@mwe.ee.ethz.ch; martin.leich@mwe.ee.ethz.ch; oolivier@phys.ethz.ch; bolognesi@mwe.ee.ethz.ch).

Color versions of one or more of the figures in this article are available online at https://doi.org/10.1109/JLT.2020.3043537.

Digital Object Identifier 10.1109/JLT.2020.3043537

This work is licensed under a Creative Commons Attribution 4.0 License. For more information, see https://creativecommons.org/licenses/by/4.0/

TABLE I
EPITAXIAL LAYER STRUCTURES

Material	Doping	Thickness
$GaAs_{0.50}Sb_{0.50}$	C : 1.2E20	20 nm
$Al_{0.17}Ga_{0.83}As_{0.55}Sb_{0.45}$	C : 5.0E19	20 nm
$GaAs_{0.50}Sb_{0.50}$	C : 1.1E18	
$GaAs_{0.50\rightarrow 0.62}Sb_{0.50\rightarrow 38}$	C : 5.2E17→3.5E18	100 nm
$Ga_{0.81}In_{0.19}As_{0.65}Sb_{0.35}$	C : 1.3E18	
InP	Si : 5.9E16	225 nm
InP	S : 3.1E19	50 nm
$Ga_{0.49}In_{0.51}As$	Si : 4.0E19	20 nm
InP	S : 3.1E19	300 nm
InP semi-insulating substrate		350 μm

in GaAs (0.284 eV), InAs (0.716 eV), GaSb (0.026 eV) and InSb (0.695 eV) also indicates that reducing the Sb- and increasing the In- mole fractions both increase the Γ-L separation in GaInAsSb with respect to GaAsSb.

We demonstrate non-graded Type-II GaInAsSb/InP UTC-PDs, and compare their performance to uniform and doping/compositionally-graded ternary GaAsSb absorber UTC-PDs fabricated on identical 225 nm thick InP collectors to outline the impact of the GaInAsSb absorber on performance. Although a clear increase in bandwidth is shown by grading GaAsSb absorbers, the uniform GaInAsSb absorber provides significant performance advantages in terms of bandwidth and photoresponse. The area dependence of PD bandwidth reveals that the enhanced transport properties of the GaInAsSb absorber enable a transit time limited cutoff frequency of 274 GHz compared to the 107 and 185 GHz bandwidths achieved with the uniform and graded GaAsSb absorbers, respectively.

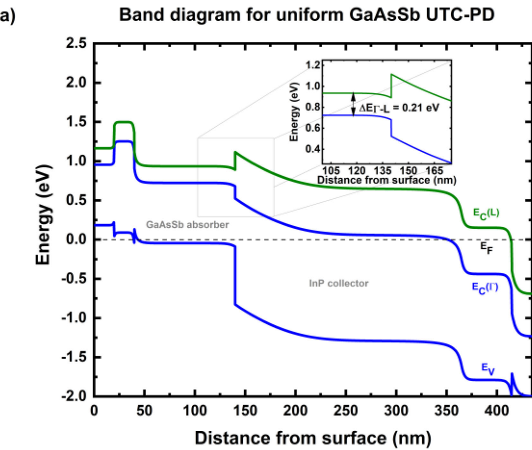

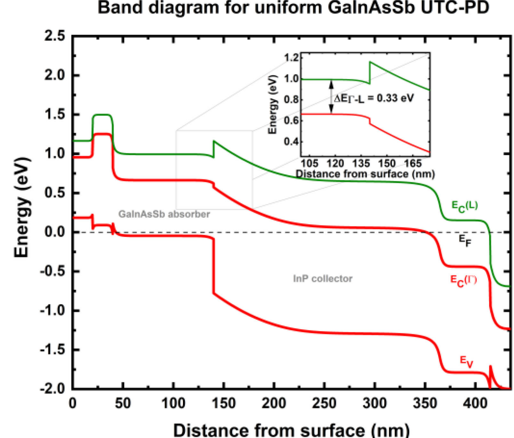

Fig. 1. Simulated equilibrium band diagrams at Γ and L point for (a) ternary GaAsSb absorber UTC-PD, and (b) quaternary GaInAsSb absorber UTC-PD. Fermi level is shown as $E_F = 0$ eV. *Insets*: Enlarged view of conduction band alignment at absorber-collector heterojunction.

II. EPITAXIAL STRUCTURES AND DEVICE FABRICATION

The three UTC-PD structures considered in the present work are shown in Table I. All designs include a 20 nm $Ga_{0.49}In_{0.51}As$ sub-collector contact layer (Si-doped at 4×10^{19} cm^{-3}), a 225 nm InP collector layer *n*-doped at 6×10^{16} cm^{-3} and a 100-nm C-doped Ga(In)AsSb based absorber. Three absorbers were compared: 1) a uniform $GaAs_{0.51}Sb_{0.49}$ absorber *p*-doped at 1.06×10^{18} cm^{-3}; 2) compositionally graded ternary $GaAs_{0.51\rightarrow 0.62}Sb$ absorber with linearly graded *p*-doping from 5.2×10^{17} cm^{-3} to 3.5×10^{18} cm^{-3}; and 3) uniform quaternary $Ga_{0.81}In_{0.19}As_{0.65}Sb_{0.35}$ absorber *p*-doped at 1.36×10^{18} cm^{-3}. All UTCs were capped with a 20 nm AlGaAsSb electron blocking layer, and a 20 nm heavily doped GaAsSb is used to form a *p*-contact for the absorber. The epitaxial layers were grown by Metal-Organic Vapor-Phase Epitaxy (MOVPE) on 2-inch semi-insulating (100) InP substrates. Fig. 1 shows simulated equilibrium band diagrams for uniform GaAsSb and GaInAsSb UTC-PDs at 300 K.

Photodiodes with sizes ranging from 64 to 200 μm^2 were fabricated by optical lithography and wet etching. An electron-beam evaporated Pd/Ni/Pt/Au *p*-contact electrode was first formed on the heavily doped GaAsSb contact layer by electron beam evaporation. The resulting contact resistivity is lower than 10^{-8} Ω-cm^2. Next, the absorber-collector (A/C) mesa structure was formed by wet etching using phosphoric acid based etching solutions. A Ti/Pt/Au *n*-contact metallization was electron beam evaporated before isolating the devices by wet etching. A SEM micrograph of a PD taken following the isolation mesa formation is shown in Fig. 2a). Finally, coplanar waveguide probe pads were electron-beam evaporated following a low-temperature (≤190 °C) Teflon based etch-back planarization process [11]. For improved responsivity, the active device area was coated with a SiN_x single layer anti-reflection coating on the top-illuminated PDs. A top-view microscope image of the completed PD is shown in Fig. 2b).

III. RESULTS AND DISCUSSION

DC characterization of UTC-PDs was performed using an HP4156B semiconductor parameter analyzer. The room temperature *I-V* characteristics show a dark current of less than 10 nA up to –5 V, as can be seen in Fig. 2c). The UTC-PD RF performance was measured from 0.2 to 60 GHz using

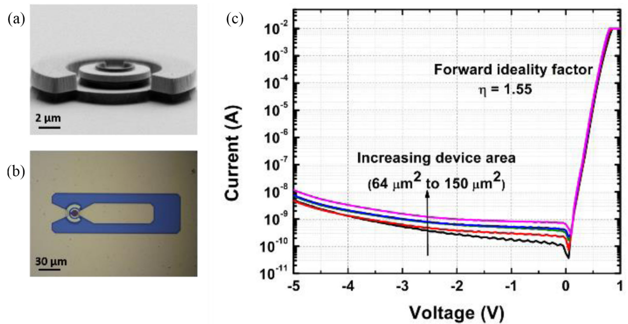

Fig. 2. (a) SEM micrograph of a UTC-PD following the isolation mesa formation; (b) Top-view microscope image of a completed UTC-PD with coplanar waveguide probe pads; (c) Dark *I-V* characteristics of GaInAsSb UTC-PDs of different areas.

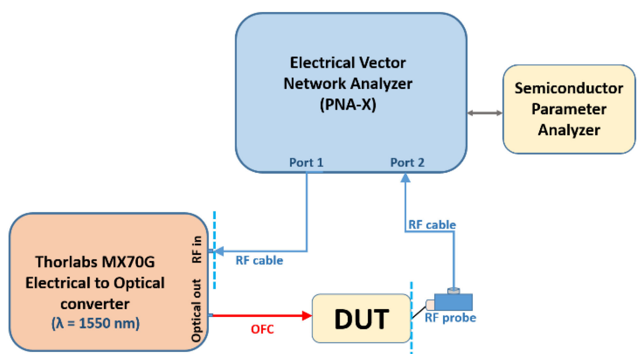

Fig. 3. Schematic diagram of the measurement setup used to characterize the UTC-PDs from 0.2 to 60 GHz. Dashed blue lines indicate the measurement reference planes.

a Thorlabs MX70G lithium niobate (LiNbO3) Mach-Zehnder modulator (MZM) electrical-to-optical converter at $\lambda = 1550$ nm and a PNA-X vector network analyzer. A schematic of the RF measurement setup is shown in Fig. 3. An off-wafer LRRM (line/reflect/reflect/match) calibration followed by de-embedding of the RF probe in port 1 brought the reference plane to the end of the RF cable in the input port, and to the RF probe tip at the output port. Dashed blue lines in Fig. 3 mark the reference planes. The modulator's frequency response was de-embedded as per [12]. A 2 mW modulated light signal at $\lambda = 1550$ nm was coupled into the top-illuminated UTC-PDs with a single-mode lensed optical fiber with a ~3 μm spot diameter.

Fig. 4 shows the S_{21} relative photoresponse plotted against frequency for GaInAsSb UTC-PDs of different sizes. Light traces represent measured data, whereas bold traces represent the equivalent circuit model fit (detailed later). Clearly, the $f_{3\text{-dB}}$ cut-off of devices is well beyond the 60 GHz measurement setup capability for devices with an area of 80 μm^2 or smaller. Fig. 5 compares the frequency response of UTC-PDs with different absorbers for two device areas. As seen from the figure, the non-graded quaternary UTC-PDs show the widest bandwidths, clearly outperforming the graded ternary absorber despite the aiding drift field associated with compositional/doping grading in the latter.

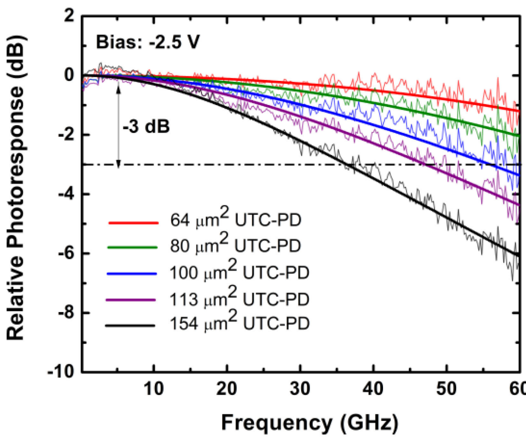

Fig. 4. Measured (thin traces) and equivalent circuit model fitted (bold traces) frequency response of GaInAsSb absorber based UTC-PDs with sizes ranging from 64 to 154 μm^2.

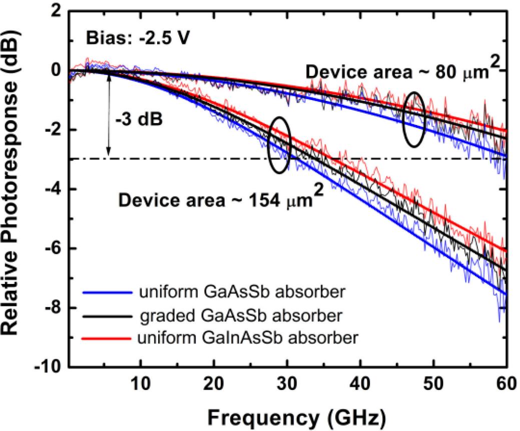

Fig. 5. Measured and equivalent circuit model fitted (bold traces) frequency responses of UTC-PDs with different absorbers for two device areas.

The two-port UTC-PD equivalent circuit model [13] shown in Fig. 6 was used to fit S_{22} and the relative S_{21} photoresponse of our devices [13]. Fitting was performed using the Keysight Advanced Design System (ADS) gradient optimizer to fit the circuit model to the measurements with minimum error goals set for i) the difference between the measured and modeled phase and magnitude of S_{22}; and ii) the difference between the measured and modeled magnitude of S_{21}. In this fashion, diode capacitances were determined to better than 1% accuracy (a 1% error in C_j produces noticeable errors in the phase of S_{22}). As the $f_{3\text{-dB}}$ cut-off frequencies are chiefly set by the junction capacitance and the 50 Ω load impedance, the extracted cut-off frequencies are very accurate. The model allows us to distinguish between the *RC*-delay and transit-delay contributions to the $f_{3\text{-dB}}$ cut-off frequencies. The fitted values for equivalent circuit elements of 80 μm^2 PDs with different absorbers are given in the table in Fig. 6. R_τ and C_τ mimic the input port frequency response roll-off due to the transit time delay of the PDs. Circuit elements in the input and output ports determine the photoresponse roll-off, while the voltage-controlled current

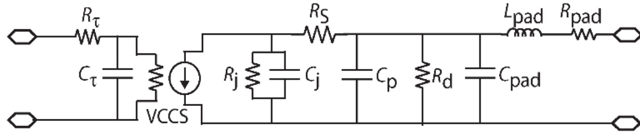

Equivalent Circuit Element	uniform GaAsSb	graded GaAsSb	uniform GaInAsSb
R_j - Diode junction resistance (kΩ)	75	75	75
C_j - Diode junction capacitance (fF)	32.5	33.5	36.4
R_S - Diode series resistance (Ω)	10.7	9.0	7.6
C_p - Diode parasitic capacitance (fF)	7.1	8.5	7.1
R_d - Pad dielectric resistance (MΩ)	0.8	0.8	0.8
C_{pad} - Pad capacitance (fF)	1.8	1.8	1.8
L_{pad} - Pad inductance (pH)	40.8	40.8	40.8
R_{pad} - Pad series resistance (Ω)	0.4	0.4	0.4

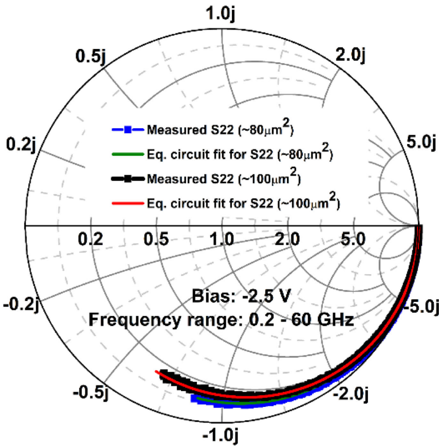

Fig. 6. (a) Equivalent circuit model used to fit the measured response of the PDs; (b) Table listing the equivalent circuit elements and their values for a 80 μm^2 PD for the three absorbers; (c) Measured and fitted S_{22} *vs.* frequency of GaInAsSb UTC-PDs for two different sizes.

source (VCCS) gain is tuned to fit the absolute response (power) level for different devices. Both measured and fitted photoresponses are then normalized near DC (0.2 GHz) value to obtain the relative photoresponse curves plotted in Figs. 4–6. The Smith chart shows the measured and fitted S_{22} for quaternary-based UTC-PDs of two different sizes, showing excellent fits to the measured data.

The measured 3-dB cutoff frequency of a PD is determined by the transit time limited bandwidth f_{T} and the RC-limited bandwidth f_{RC} as:

$$\frac{1}{f_{3dB}^2} = \frac{1}{f_{RC}^2} + \frac{1}{f_T^2} = (2\pi RC)^2 + \frac{1}{f_T^2} \tag{1}$$

where R is the sum of the PD series resistance and the load resistance of 50 Ω, and C is the PD capacitance inclusive of the junction capacitance at bias and the parasitic capacitance. Plotting measured data according to Eqn. (1) and extrapolating to $RC = 0$ yields the transit-limited UTC-PDs bandwidth f_{T}.

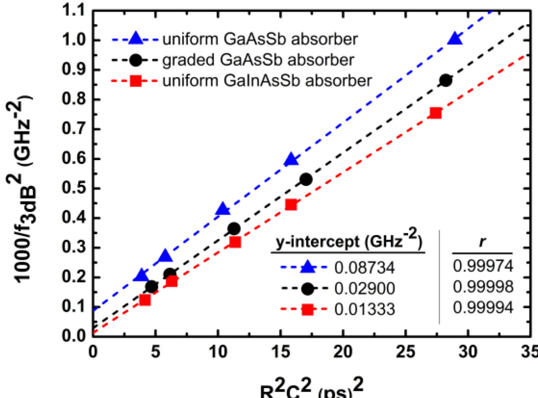

Fig. 7. $1000/f_{3dB}^2$ plotted against R^2C^2 for UTC-PDs with three different absorbers. Linear extrapolation to $RC = 0$ determines the transit limited bandwidth for each of the PDs. The y-intercept value and the linear correlation coefficient r are shown.

Using the equivalent circuit model, the extracted overall 3-dB bandwidth is plotted as $(1000/f_{\mathrm{3dB}}^2)$ against the RC delay as shown in Fig. 7 for all absorber types. In all cases, the linear regression coefficient $r > 0.9997$, demonstrating the robustness of the extraction procedure. A transit time limited cutoff frequency of $f_{\mathrm{T}} = 274$ GHz is extracted for the GaInAsSb absorber, compared to 107 and 185 GHz for the uniform and graded GaAsSb absorbers, respectively. Fig. 7 also shows that our large area devices are RC-limited, and that significant improvements in 3-dB bandwidth can be achieved by area scaling, especially with GaInAsSb absorbers.

The 2.58× improvement of transit time limited cutoff frequency f_{T} for GaInAsSb over GaAsSb -based UTC-PDs follows from improved electron transport in the quaternary alloy. The minority electron mobility in p-type GaInAs was reported to be higher than in GaAsSb for any given doping concentration [7]. It is reasonable to anticipate an increased electron mobility with Indium incorporation into GaAsSb, as verified by Flückiger *et al.* [14]. Because Γ-valley electron effective masses for lattice-matched GaInAs and GaAsSb are very similar, the improved electron transport in the quaternary GaInAsSb alloy is not simply due to a higher electron mobility in the Γ-valley. By means of experiments supported by quantum transport simulations, Bolognesi *et al.* [10] showed that the improvement in the electron transport properties arises from a higher Γ-L valley separation. The Γ-L valley separation in GaAsSb absorbers is $\Delta E_{\Gamma\text{-L}} = 0.21$ eV, whereas, $\Delta E_{\Gamma\text{-L}} = 0.33$ eV for the quaternary absorber [15], as shown in Fig. 1. At room temperature, the percentage of electrons in the slower L-valley is thus significantly higher in GaAsSb compared to GaInAsSb. L-valley population should be minimized in light of its blocking Type-I transition between absorber and the InP collector (which impedes collection of L-valley electrons).

Beside improvements in bandwidth, GaInAsSb absorbers also result in a higher PD responsivity. Table II shows measured responsivities for large area UTC-PDs with different absorbers

TABLE II
EXTERNAL RESPONSIVITY* AND TRANSIT-LIMITED-BANDWIDTH OF THE UTC-PDS

	Uniform GaAsSb Absorber	Graded GaAsSb Absorber	Uniform GaInAsSb Absorber
Responsivity (A/W)	0.070	0.062	0.094
f_T (GHz)	107	185	274

*Measured on large area devices.

under study. GaInAsSb quaternary absorbers show a 34% responsivity improvement with respect to GaAsSb. The responsivity of the graded GaAsSb absorber is reduced because of a reduced carrier lifetime due to higher doping, and a wider energy gap for As concentrations >50%. The higher responsivity of GaInAsSb absorbers can be attributed to: i) the narrower bandgap in $Ga_{0.81}In_{0.19}As_{0.65}Sb_{0.35}$ compared to GaAsSb; ii) reduced carrier recombination in the absorber thanks to a reduced transit time; iii) a relatively lower population of electrons in the absorber L-valley (reduced blocking to InP); and iv) a longer Auger recombination lifetime of in GaInAsSb relative to GaAsSb [16]. Further experiments are needed to determine which factor, if any, dominates. The 94 mA/W responsivity of the 100 nm GaInAsSb absorber compares well to the 126 mA/W achieved in Ito *et al.* with a two-pass (back-illuminated with topside reflector) 86 nm thick GaInAs absorber and a 230 nm InP collector [17]. In [17] a cutoff frequency of 235 GHz (τ_{3dB} = 0.68 ps) was achieved for a 13 μm^2 diode area. The scaling relation of Eqn. (1) for the GaInAsSb absorber indicates an f_{3dB} = 240 GHz (τ_{3dB} = 0.66 ps) for a 13 μm^2 area despite a 16% thicker absorber layer, suggesting that diffusive electron transport in our GaInAsSb absorber indeed is competitive with that of GaInAs. Because the present InP collector is nearly of the same thickness as that of [17], by accounting for a collector delay $\tau_C = 0.26$ ps [6, 10] and the *RC* delay per Eqn. (1), we relate the effective mobilities of electrons in the GaInAsSb and GaInAs absorbers, μ_Q and μ_{GaInAs}, to the ratio of absorber delay times $\tau_{A,GaInAs} = 0.337$ ps and $\tau_{A,Q} = 0.321$ ps as

$$\left(\frac{0.337}{0.321}\right) \cdot \left(\frac{W_{A,Q}}{W_{GaInAs}}\right)^2 = \left(\frac{0.337}{0.321}\right) \cdot \left(\frac{100}{86}\right)^2 = \left(\frac{\mu_Q}{\mu_{GaInAs}}\right) = 1.42.$$

Assuming responsivity scales with absorber layer thickness and mobility [6] (recalling the effective absorber length in [17] is 172 nm for two-passes through the 86 nm GaInAs layer), yields μ_Q/μ_{GaInAs} = (94·172)/(126·100) = 1.28, which is consistent with the value extracted from bandwidth comparison (with an ~11% discrepancy that is likely associated to a higher recombination rate due to the 6.5× higher doping level in our GaInAsSb absorber with respect to that of [17]).

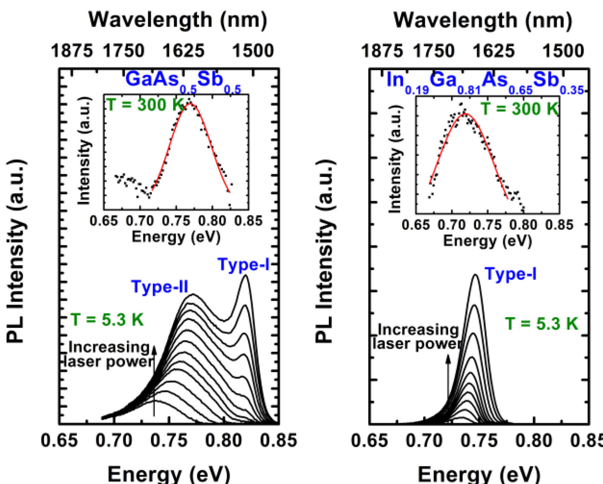

Fig. 8. Low-temperature (5.3 K) photoluminescence spectra for 100 nm thick $GaAs_{0.50}Sb_{0.50}$ and $Ga_{0.81}In_{0.19}As_{0.65}Sb_{0.35}$. Type-I denotes the transition across bandgap and Type-II represents the Type-II transition at the interface between the material and InP. *Inset*: corresponding room temperature PL spectra.

The bandgap calculation for the ternary and quaternary III-V alloys depends on both the selected interpolation scheme and the bowing parameters. For example, the calculated energy gap for $Ga_{0.81}In_{0.19}As_{0.65}Sb_{0.35}$ varies from 0.70 eV [18] to 0.81 eV [15]. Photoluminescence (PL) measurements were performed on the ternary and quaternary absorber alloys to experimentally determine the bandgaps and the conduction band offsets to InP at the A/C junction. Fig. 8 shows the PL data measured at 5.3 K for GaAsSb and GaInAsSb on non-intentionally doped InP. The optical pumping power was varied from 3.93 to 15.72 mW/cm^2 in steps of 1.31 mW/cm^2 for the quaternary absorber. For the ternary absorber, the pumping power was varied from 6.55 to 15.72 mW/cm^2, first in steps of 1.31 mW/cm^2 and then in steps of 0.66 mW/cm^2 once the Type-I peak appears (it is quenched under low laser excitation because electron diffusion to the InP collector competes with radiative recombination in GaAsSb by lowering the excess electron density). A Type-II (spatially indirect) transition peak is visible for GaAsSb but not for GaInAsSb. This indicates that In- incorporation lowers the conduction band edge of GaInAsSb until it nearly aligns with that of InP. Calculations as per [15] show that an In- mole fraction in excess of 20% results in a blocking Type-I transition with InP and justifies the choice of a 19% In-mole fraction in our quaternary absorber. The PL measurements also confirm a lower energy gap for GaInAsSb which lends itself to an improved responsivity with respect to GaAsSb. Room temperature PL data (Fig. 8 insets) indicate energy bandgaps of $E_G = 0.77$ and 0.71 eV for GaAsSb and GaInAsSb, respectively.

The transit time limited cut-off of our quaternary UTC-PDs can be further improved by composition and/or doping grading schemes, and by reducing their area. The present study highlights the interest of GaInAsSb absorbers in UTC-PDs based on simple top-illuminated structures, future work will improve the overall responsivity with resonant cavity structures and/or conversion to a waveguide architecture [19], [20]. Significant

improvements in responsivity are expected since optical electromagnetic simulations for the present UTC-PD demonstrators show that the peak optical field region is not aligned with the absorber layers.

IV. Conclusion

We demonstrated the first quaternary GaInAsSb absorber Type-II UTC-PDs and compared their properties to GaAsSb –based PDs (all with 100 nm absorbers). The extracted transit limited bandwidth of our GaInAsSb UTC-PDs is $f_T = 274$ GHz in comparison 185 GHz for graded GaAsSb PDs, and 107 GHz for uniform GaAsSb PDs with the same absorber thickness (2.58× improvement for non-graded structures). The GaInAsSb absorbers also yield a 34% higher responsivity compared to the best GaAsSb absorber considered. Scaling down the active device area and a graded GaInAsSb absorber can still greatly increase the overall bandwidth of the PDs in comparison to the GaAsSb UTC-PDs.

A performance comparison to GaInAs-based UTC-PDs with similar layer thicknesses suggests that In- incorporation in GaAsSb not only makes its properties competitive to those of GaInAs, but that it indeed results in superior absorber material properties for high-speed photodetector applications at $\lambda = 1.55\ \mu$m. We consider this finding about the GaInAsSb alloy to be of importance because it was heretofore held that the "*usefulness of this quaternary is limited because both end points have nearly the same energy gap*," as per [15].

Acknowledgement

The authors would like to thank the staff of FIRST Lab at ETH Zurich, Zurich, Switzerland, for their support.

References

[1] H. Ito, T. Furuta, S. Kodama, T. Ishibashi, "InP/InGaAs uni-travelling-carrier photodiode with 310 GHz bandwidth," *Electron. Lett.*., vol. 36, no. 21, pp. 1809–1810, Oct. 2000.

[2] T. Ishibashi, Y. Muramoto, T. Yoshimatsu and H. Ito, "Unitraveling-carrier photodiodes for terahertz applications," *IEEE J. Sel. Top. Quantum Electron.*, vol. 20, no. 6, Nov.-Dec. 2014, Art. no. 3804210.

[3] T. Nagatsuma, G. Ducournau, and C. Renaud, "Advances in terahertz communications accelerated by photonics," *Nat. Photon.*, vol. 10, pp. 371–379, 2016.

[4] E. Rouvalis, M. J. Fice, C. C. Renaud and A. J. Seeds, "Millimeter-wave optoelectronic mixers based on uni-traveling carrier photodiodes," *IEEE Trans. Microw. Theory Techn.*, vol. 60, no. 3, pp. 686–691, Mar. 2012.

[5] C. Nguyen, T. Liu, M. Chen, H-C. Sun and D. Rensch, "AlInAs/GaInAs/InP double heterojunction bipolar transistor with a novel base-collector design for power applications," *IEEE Electron. Device Lett.*, vol. 17, no. 3, pp. 133–135, Mar. 1996.

[6] L. Zheng *et al.*, "Demonstration of high-speed staggered lineup GaAsSb-InP unitraveling carrier photodiodes," *IEEE Photon. Technol. Lett.*, vol. 17, no. 3, pp. 651–653, Mar. 2005.

[7] W. Tea and F. Aniel, "Minority electron mobilities in GaAs, In0.53Ga0.47As, and GaAs0.50Sb0.50 calculated within an ensemble monte carlo model," *J. Appl. Phys.*, vol. 109, no. 3, Feb. 2011, Art. no. 033716.

[8] A. Dyson, I. D. Henning and M. J. Adams, "Comparison of Type I and Type II heterojunction unitravelling carrier photodiodes for terahertz generation," *IEEE J. Sel. Top. Quantum Electron.*, vol. 14, no. 2, pp. 277–283, Mar.-Apr. 2008.

[9] W. Quan, A. M. Arabhavi, R. Flückiger, O. Ostinelli, and C. R. Bolognesi, "Quaternary graded-base InP/GaAsSb DHBTs with $f_T/f_{MAX} =$ 547/784 GHz," *IEEE Electron Device Lett*., vol. 39, no. 8, pp. 1141–1144, Aug. 2018.

[10] C. R. Bolognesi *et al.*, "Advances in InP/Ga(In)AsSb double heterojunction bipolar transistors (DHBTs)," *Jpn. J. Appl. Phys*, vol. 58, Mar. 2019, Art. no. SB0802.

[11] R. Flückiger, R. Lövblom, O. Ostinelli, H. Benedickter, and C. R. Bolognesi, "InP/GaAsSb DHBTs fabricated in a low-temperature teflon planarization process," *IEEE Electron Device Lett*., vol. 33, no. 8, pp. 1135–1137, Aug. 2012.

[12] "De-embed application note for Thorlabs MX40/70G calibrated electrical-to-optical converter," May 16, 2017. [Online]. Available: https://www.thorlabs.com/images/TabImages/MX40G_De-Embed_Procedures.pdf

[13] J. Wun, R. Chao, Y. Wang, Y. Chen and J. Shi, "Type-II GaAsb0.5Sb0.5/InP uni-traveling carrier photodiodes with sub-terahertz bandwidth and high-power performance under zero-bias operation," *J. Lightw. Technol.*, vol. 35, no. 4, pp. 711–716, Feb. 2017.

[14] R. Flückiger, R. Lövblom, M. Alexandrova, O. Ostinelli, and C. R. Bolognesi, "Uniform-base InP/GaInAsSb DHBTs exhibiting $f_{MAX}/f_T =$ 635/420 GHz," *IEEE Electron Device Lett*., vol. 35, no. 2, pp. 166–168, Jan. 2014.

[15] I. Vurgaftman, J. R. Meyer, and L. R. Ram-Mohan, "Band parameters for III-V compound semiconductors and their alloys," *J. Appl. Phys.*, vol. 89, no. 11, pp. 5815–5875, Jun. 2001.

[16] S. Chen, C. Chang, P. Chiang, S. Wang, W. Chang and J. Chyi, "DC characteristics of InAlAs/InGaAsSb/InGaAs double heterojunction bipolar transistors," *IEEE Trans. Electron. Devices*, vol. 57, no. 12, pp. 3327–3332, Dec. 2010.

[17] H. Ito, T. Furuta, S. Kodama, N. Watanabe and T. Ishibashi, "InP/InGaAs uni-travelling-carrier photodiode with 220 GHz bandwidth," *Electron. Lett.*, vol. 35, no. 18, pp. 1556–1557, Sep. 1999.

[18] K. Shim, H. Rabitz, and P. Dutta, "Band gap and lattice constant of $\text{GaxIn}_1-\text{xAsySb}_{1-y}$," *J. Appl. Phys.* vol. 88, no. 12, pp. 7157–7161, 2000.

[19] K. Kishino, M. S. Unlu, J.-I. Chyi, J. Reed, L. Arsenault and H. Morkoc, "Resonant cavity-enhanced (RCE) photodetectors," *IEEE J. Quantum Electron.*, vol. 27, no. 8, pp. 2025–2034, Aug. 1991.

[20] T. Umezawa, K. Akahane, A. Matsumoto, A. Kanno, N. Yamamoto, and T. Kawanishi, "High-responsivity 100 GHz waveguide UTC photodetector," in *Proc. Broadband Access Commun. Technol.*, 2017, Art. no. 1012807.